LARGE-SCALE SOLAR VELOCITY FIELDS

THOMAS L. DUVALL, Jr.*
Institute for Plasma Research, Stanford University, Stanford, Calif. 94305, U.S.A.

(Received 17 July, 1978; in final form 8 March, 1979)

Abstract. Daily observations of Doppler line shifts made with very low spatial resolution (3′) with the Stanford magnetograph have been used to study the equatorial rotation rate, limb effect on the disk, and the mean meridonial circulation. The equatorial rotation rate was found to be approximately constant over the interval May 1976–January 1977 and to have the value 2.82 μrad s^{-1} (1.96 km s^{-1}). This average compares favorably with the results of Howard (1977) of 2.83 μrad s^{-1} for the same time period. The RMS deviation of the daily measurements about the mean value was 1% of the rate (20 m s^{-1}), much smaller than the fluctuations reported by Howard and Harvey (1970) of several per cent. These 1% fluctuations are uncorrelated from day-to-day and may be due to instrumental problems. The limb effect on the disk was studied in equatorial scans (after suppressing solar rotation). A redshift at the center of the disk relative to a position $0.60R_\odot$ from the center of 30 m s^{-1} was found for the line Fe I λ5250 Å. Central meridian scans were used (after correcting for the limb effect defined in the equatorial scans) to search for the component of mean meridonial circulation symmetric across the equator. A signal is found consistent with a polewards flow of 20 m s^{-1} approximately constant over the latitude range 10–50°. Models of the solar differential rotation driven by an axisymmetric meridonial circulation and an anisotropic eddy viscosity (Kippenhahn, 1963; Cocke, 1967; Köhler, 1970) predict an equatorwards flow at the surface. However, giant cell convection models (Gilman, 1972, 1976, 1977) predict a mean polewards flow (at the surface). The poleward-directed meridonial flow is created as a by-product of the giant cell convection and tends to limit the differential rotation. The observation of a poleward-directed meridonial circulation lends strong support to the giant cell models over the anisotropic eddy viscosity models.

1. Introduction

Full-disk measurements of Doppler line shifts were made beginning in May 1976 as a part of the daily magnetogram observation at Stanford. These observations, in conjunction with measurements of the mean (integrated light) solar magnetic field (Scherrer *et al.*, 1977), are the main components of an observing program whose goal is to observe the large-scale magnetic and velocity fields on a synoptic basis for at least one solar cycle. In this paper the doppler shift measurements are used to study the equatorial rotation rate and the limb effect on the disk. Pole-to-pole scans along the central meridian were made at the end of each day's magnetogram beginning in July 1976. These data are used to search for a mean meridonial circulation.

2. Description of Experiment

The telescope light path is shown in Figure 1. A two-mirror coelostat system feeds the telescope. The (non-rotating) solar image formed at the spectrograph entrance

* Now at Kitt Peak National Observatory, Tucson, Ariz., U.S.A.

Solar Physics **63** (1979) 3–15. 0038–0938/79/0631–0003 $01.95.

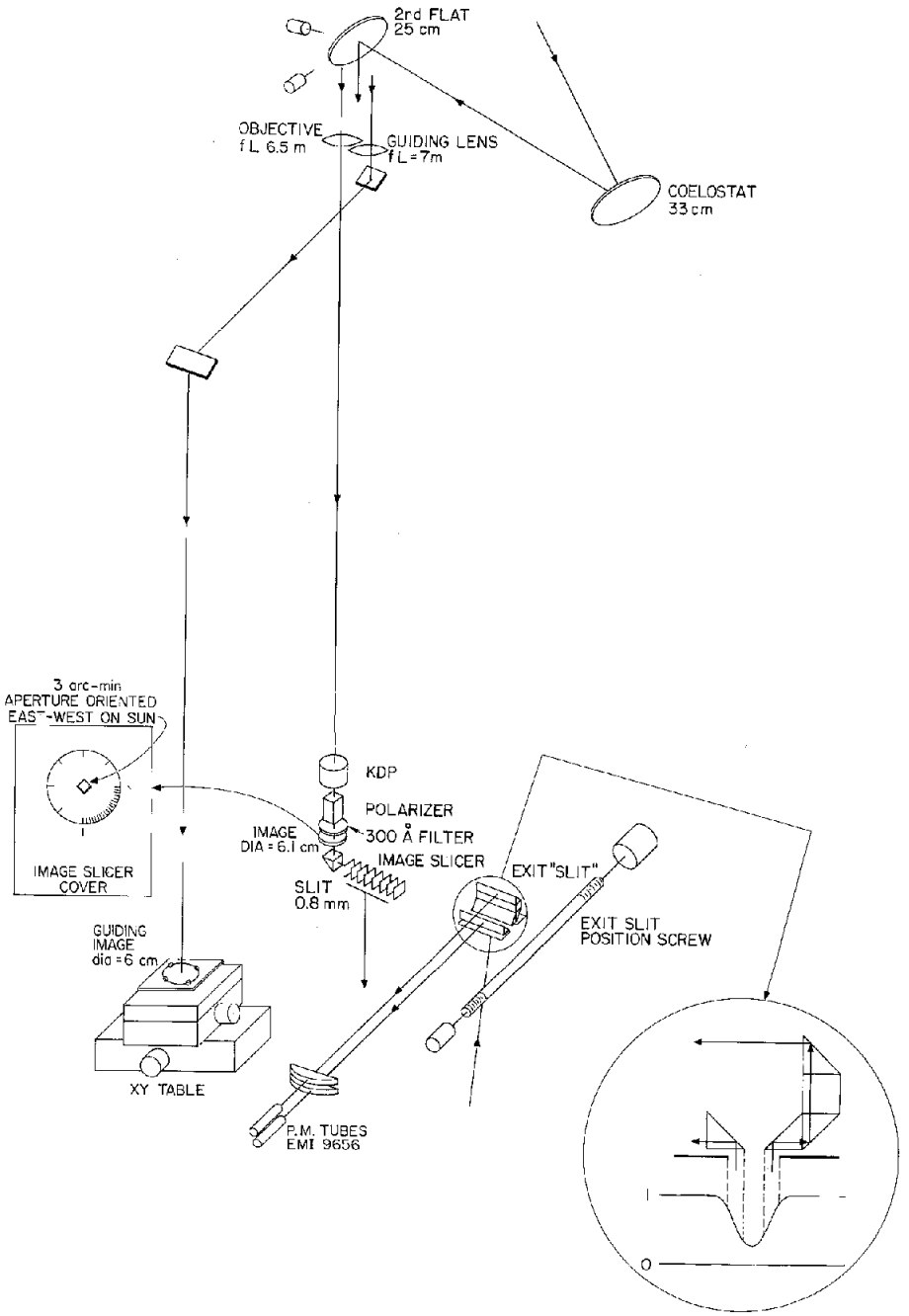

Fig. 1. Telescope light path. The spectrograph is not shown.

slit has a 6.1 cm diameter. Coarse guiding is provided by the rotation of the main coelostat mirror by a clock-driven motor. A secondary beam, used for fine guiding and image positioning, forms an image at ground level. At the position of the secondary image two matched pairs of photodiodes are mounted on an x-y positioning table at opposite limb points. An analog servo system, whose error is the difference signal between a pair of photodiodes at opposite limb-points, controls the position of the second flat mirror to keep the image centered on the photodiodes. The main solar image is positioned relative to the entrance aperture by movement of the x-y positioning table table by computer-controlled stepper motors (1 step = 0.001 in.).

Analyzing optics before the entrance aperture are a modulated circular polarization analyzer (KDP crystal and linear polarizer) and a 300 Å bandpass interference filter to suppress overlapping orders from the grating. The square entrance aperture (~3′ on a side) is oriented east–west in solar coordinates. The square aperture is converted to the slit geometry (spectrograph entrance slit = 0.8 mm × 100 mm) by an image slicer. The spectrograph is of the vertical Littrow type with focal length 22.4 m. The Littrow lens has a clear aperture of diameter 6 in. The Babcock grating is 6 in. × 13 in., has 633 lines mm^{-1} and is blazed for observation in the fifth-order green. The dispersion in the exit slit plane is ~ 13 mm $Å^{-1}$ in the fifth-order green.

The exit slit apparatus is similar to the one at the Mt. Wilson 150-foot tower telescope (Howard and Harvey, 1970). The exit slits consist of a pair of prisms whose illumination is controlled by adjustable blinds placed in front of the prisms (Figure 1). The light from the exit slits is focused on to a pair of EMI 9656 photomultiplier tubes by Fabry lenses. The exit slit prisms are mounted on ways that are positioned by a finely machined screw. The screw is linear to within 5 m s^{-1} over a displacement corresponding to solar rotation. A Fraunhofer absorption line is kept centered on the exit slits by an analog servo system which controls the position of the screw. Doppler shifts are observed by measuring the rotation of the screw with a shaft encoder (1 count = 2.75 m s^{-1}). The spectral line used is Fe I λ5250 Å. The exit slit widths are 75 mÅ and their separation is 18 mÅ.

A stepping mode is used to make the full-disk magnetogram. The image is stepped in the east–west (in solar coordinates) direction by 1.5′ and the magnetic, velocity, and intensity signals integrated for 15 s. Successive east–west swaths are separated by 3′ in the north–south (solar) direction.

The central meridian observations are made by stepping the solar image from south to north (stepsize 3′) and then from north to south so that linear instrumental drifts can be cancelled by averaging the two observations. The same integration time is used (15 s).

The velocity signals are calibrated by measuring with the exit slit apparatus the wavelength separation of two spectral lines. The first step in the data reduction is to correct the velocity signal for the motion of the observatory relative to the Sun by the method described by Howard and Harvey (1970).

3. Analysis and Discussion

3.1. Equatorial rotation rate

The results of one day's full-disk velocity measurements are shown as a contour plot in Figure 2. The almost parallel contours of equal line-of-sight velocity are indicative of the solar rotation. Also visible are systematic effects near the limbs of both solar (limb-effect) and instrumental (discussed below) origin. The data from the central swath have been used to derive the equatorial rotation rate. Because of the irregularities at the limbs, only data within $0.6R_\odot$ of disk center are considered. A plot of the line-of-sight velocity for the central swath as a function of distance across the disk is shown in Figure 3.

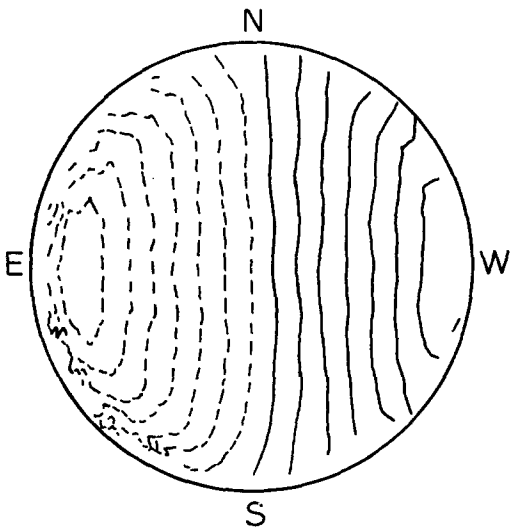

Fig. 2. Contour plot of the line of sight velocity signal observed on June 18, 1976. The contour levels are $\pm 100, 300, \ldots$ m s^{-1}. These are the raw data before any corrections are applied.

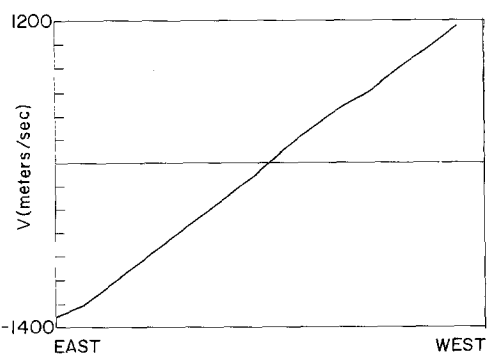

Fig. 3. Example of the line of sight velocity measured along the central swath for one day's observation. The data are shown only to $0.6R_\odot$ from disk center.

To derive the rotation rate, consider the geometry as shown in Figure 4. The linear velocity of solar rotation at latitude λ is $\omega R_\odot \cos\lambda$, where ω is the angular velocity ($\omega = \omega(\lambda)$). The line-of-sight component of this velocity, in the case that the rotation axis is not inclined toward the observer, is $\omega R_\odot \cos\lambda \sin\phi$ (ϕ = longitude measured from central meridian). When the rotation axis is inclined toward the observer, the line-of-sight velocity is

$$V_{sr} = \omega R_\odot \cos\lambda \sin\phi \cos\lambda_0, \tag{1}$$

where λ_0 is the heliocentric latitude of disk center ($\cos\lambda_0$ varies throughout the year within the range 0.992–1.000). $\sin\phi$ is linear across the disk resulting in the linear dependence of line-of-sight velocity seen in Figures 2 and 3. The data from the central swath have been fitted by least-squares to the above expression to find a rotation rate ω. Due to the inclination of the rotation axis toward the observer, the central swath data do not correspond precisely to the equator. However, the differential rotation is small in the region near the equator and so the results are indicative of the equatorial rotation rate. λ and ϕ have been calculated from instrumental parameters by the method described by Howard and Harvey (1970).

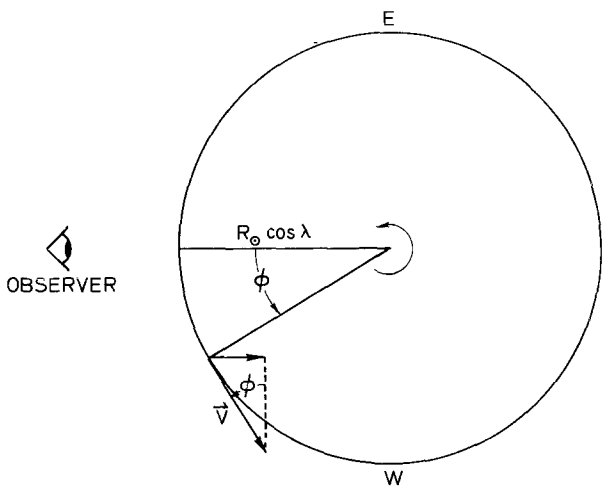

Fig. 4. Geometry for the velocity signal. The latitude circle λ is shown. ϕ is the longitude measured with respect to the central meridian. Velocities are defined as positive going away from the observer.

The derived values for the equatorial rotation rate as a function of time for the second half of 1976 are shown in Figure 5. The rate is roughly constant over this interval and the average value is 2.77 μrad s^{-1}. Two systematic errors need to be considered:

(1) During most of the time interval there was a systematic drift during each observation of the velocity signal due to a residual motion of the grating, which was set before the observation. The drift was mostly in the same direction in each day's

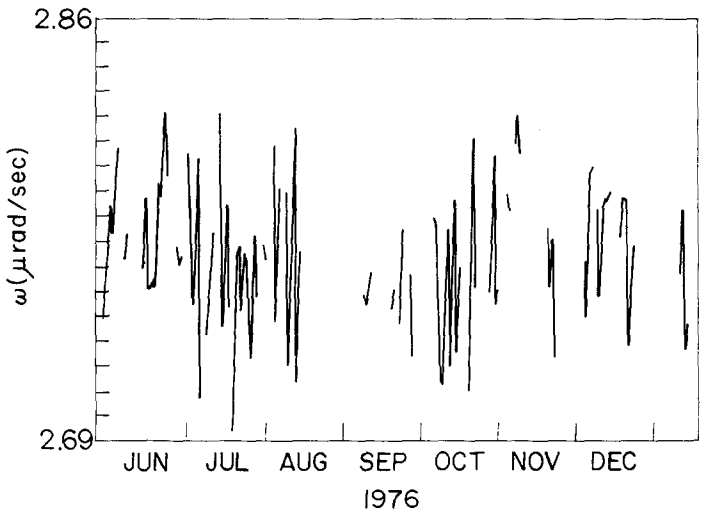

Fig. 5. The equatorial rotation rate as a function of time during the second half of 1976. Each point represents a fit to the data of the central swath (data are only used to $0.6R_\odot$ from disk center) for one day's observation. The points are connected when adjacent days have data. Tables of the daily values are available upon request.

observation and was measured by observing the velocity signal at the center of the disk both before and after the observation. The central swath was always traversed in the same direction, resulting in an error in the average rotation rate. The drift was not linear during the observation and so a direct interpolation could not be used to correct it. However, successive east–west swaths are traversed in opposite directions and hence have errors of opposite sense. By comparing the rates computed from adjacent swaths, a correction of 0.01 μrad s^{-1} was found that should be added to the rate shown above.

This drift is thought to be caused by a mechanical problem with the grating rotation. It was found that after the grating was rotated from one spectral position to another a strong drift of the spectrum occurred ($\sim$400 m s^{-1} in 10 min). This drift decayed in time so that 30 min after the grating had been rotated the drift had decreased $\sim$100 m s^{-1} h^{-1}. This drift was known to be present at the time of the beginning of the present observations. Before each observation the grating was rotated to the nonmagnetic line Fe I λ5124 Å to determine the magnetic zero offset. The grating was then rotated back to the λ5250 Å position. For the first month's observations we then waited 15 min before starting the full-disk observation (to give the grating drift time to decay). After one month's observations it was decided that 15 min was not long enough to wait and a 30 min waiting period was introduced. After three months of observation a method was found to correct for the grating drift. The grating was driven (by electric motor) near its desired position and then for a few seconds the motor direction was reversed. This solved the problem of the large drift after grating rotation. Later measurements of spectral drift indicated a value

near 60 m s^{-1} h^{-1}. Whether this is due to residual grating motion or other causes is not known.

(2) The need for another correction is shown in Figure 6, which is a plot of the average rotation rate computed using only two points placed symmetrically about disk center as a function of distance from the center. The apparent decrease of the rotation rate for points away from disk center is surely an instrumental effect, which is supported by measurements with a telluric line showing an apparent rotation opposite to the solar rotation. The effect is probably caused by the limb darkening along the long (10 cm) entrance slit coupled with a misalignment in the spectrograph. The correction is derived by extrapolating the points of Figure 6 to the center of the disk, resulting in an equatorial rate of 2.81 μrad s^{-1}. The point near $r/R_\odot = 0.1$ has been disregarded because its error is much larger than the other points in Figure 6. Adding the drift correction yields a final result of 2.82 μrad s^{-1}. This result compares favorably with the average rate of 2.83 μrad s^{-1} derived from Mt. Wilson measurements for the same time period (Howard, 1977).

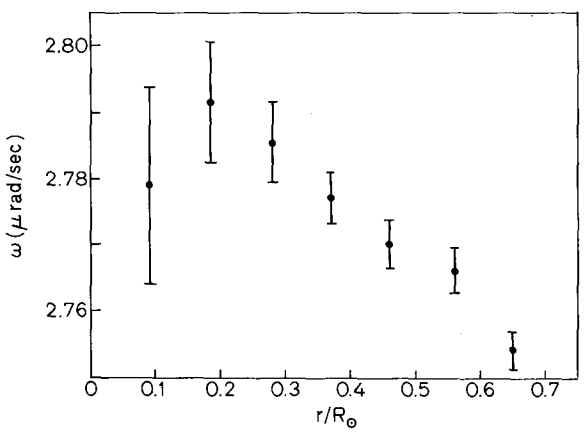

Fig. 6. Computed rotation rates as a function of distance from disk center. Each point represents the average rate for the second half of 1976 computed using only two datapoints placed symmetrically about the disk center. The variation is assumed to be of instrumental origin (see text).

Howard and Harvey (1970) reported variations of the equatorial rotation rate of several per cent on time time scales of days to weeks to months. The results of Figure 5 do not show such variations. The RMS deviation about the mean of the rates is 1% of the average (20 m s^{-1}). These deviations are uncorrelated from one day to the next (the autocorrelation function falls to zero at a lag of one day). Some of these deviations (and possibly all) are caused by instrumental drifts and small-scale solar velocity fields. It is concluded that any variations of the equatorial rotation rate during this time interval were <20 m s^{-1}.

Recent work (Svalgaard *et al.*, 1979) has shown the importance of proper correction of scattered light. The main effect is a decrease by several percent of the

measured rotational velocity. None of the data reported in the present paper have been corrected for scattered light thus ensuring comparability with other observers.

3.2. Limb effect on the disk

The limb effect can be defined as a line shift which, as a function of position on the apparent disk, is only a function of the distance from the center. This line shift is superposed on other solar line shifts (rotation, gravitational redshift, local velocity fields, etc.) but can be extracted by suitable analysis. The name limb effect is used because most of the variation in wavelength of the line occurs very near the limb. Howard and Harvey (1970) found a redshift at the limb relative to disk center of 300 m s^{-1} for the line Fe I λ5250 Å where most of the variation occurs within 2′ of the limb.

The low spatial resolution of the present observations precludes the study of the limb effect near the limb. However, it can be studied on the disk using the data of the central swath. For each day's data rotation is suppressed by using the fitted rotation rate to compute velocity residuals $\Delta V = V_{\text{meas}} - V_{\text{sr}}$ as a function of distance across the disk. The zero point of the residuals is arbitrary because of the lack of a wavelength reference. It is set by requiring the sum of the residuals to be zero. Local velocity fields, instrumental noise and possible large-scale convection are suppressed by averaging the residuals over a number of solar rotations. The limb-effect will appear in the average residuals as a velocity signal which is symmetric across the central meridian.

Average residuals for several solar rotations are shown in Figure 7. The average is compared with observations made on three separate days, in which the central swath was repeatedly scanned to lower the noise level. The main effect present in the average and on the single days is symmetric about the disk center and is a redshift at the center relative to a distance $0.60R_{\odot}$ from the center of 30 m s^{-1}. The slight asymmetry about central meridian is caused by the instrumental effect described in the previous section in which for points farther from central meridian a slower rotation is measured. The part of the signal of Figure 7 symmetric about central meridian cannot be caused by an average photospheric flow velocity, for (i) an average east–west horizontal motion would be suppressed by the solar rotation analysis, (ii) horizontal north–south motions are perpendicular to the line of sight, and (iii) an average vertical velocity large enough to yield this signal would result in an unacceptably high flux of matter across the photosphere. The signal is therefore interpreted as a manifestation of the limb effect on the disk, with its source either correlations of velocity and intensity of unresolved photospheric features or pressure shifts. The pressure shift hypothesis (Hart, 1974) seems an unlikely cause in this case because of the small variation in the height of formation of the 5250 Å line over the region studied (Lites, 1972).

By comparing the three single days' residuals with the average in Figure 7, it is possible to put an upper limit to the magnitude of the signal resulting from large-scale convection of 10 m s^{-1} for this small sample of observations.

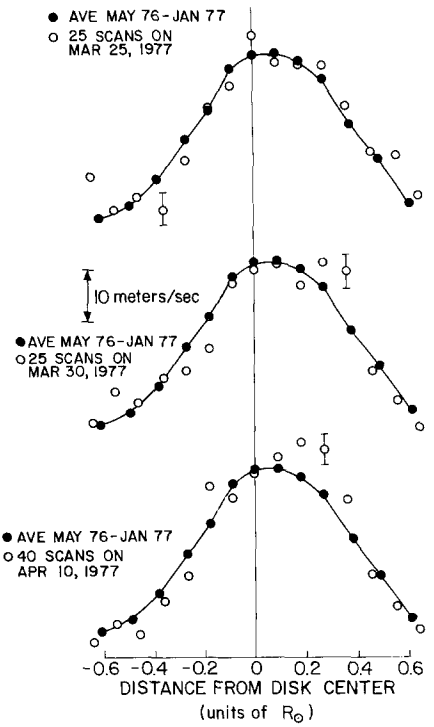

Fig. 7. Average velocity residuals (central swath) for several rotations (●) compared with residuals computed from scans made on three single days (○). The error bars for the several rotation average are ~ 1 m s^{-1}.

The limb effect shows quite a different behavior for different lines. Howard (1972) found that the redshift at the limb relative to the center for the line λ5233 Å of Fe I was ~ 800 m s^{-1}. The limb effect on the disk was studied for λ5233 Å by repeated scanning of the central swath on a single day and then computing velocity residuals as described previously. The results are shown in Figure 8, in which the λ5233 Å observations are compared with λ5250 Å observations made on the same day. The limb effect on the disk for the λ5233 Å line has quite a different behavior, showing a redshift at $0.65R_\odot$ relative to disk center of ≈ 70 m s^{-1}.

3.3. Meridional Circulation

Given that the limb effect on the disk has been defined, it is possible to search for meridional circulation using the data of the scans made along the central meridian. The reason for looking along the central meridian is that rotation is perpendicular to the line-of-sight and therefore does not enter. Because of instrumental errors (small position angle errors inducing a component of solar rotation and an error similar to the one causing decreased solar rotation toward the limb) which are asymmetrical across disk center, it was decided to look for the component of meridional circulation symmetric about the equator by folding the central meridian scans across disk center.

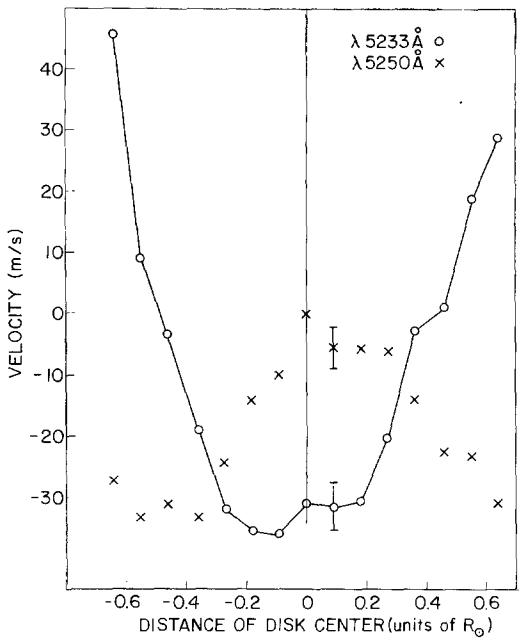

Fig. 8. Velocity residuals for the central swath for the lines λ5250 Å and λ5233 Å of Fe I observed on the same day. The exit slits used for the λ5233 Å line were the same width and separation as for the λ5250 Å line.

The center of the disk does not always correspond to the solar equator and this was taken into account by averaging data for approximately one year. To cancel the slight asymmetry across central meridian in the east–west residuals, the limb effect on the disk was defined by folding the residuals across central meridian. The average folded central meridian scan is compared with the average residuals in Figure 9. The two

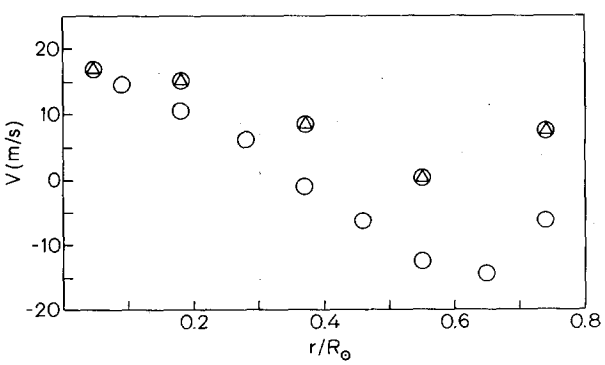

Fig. 9. Average folded velocity residuals (○) for the central swath compared with the average folded central meridian scan (◬). All folding is done across the center of the disk. Disk center is at the left in the plot. The two groups of points have been shifted vertically so they match at disk center. 171 central swath residuals and 184 central meridian scans during the time period July 20, 1976–June 22, 1977 went into the averages. The computed errors are < 1 m s^{-1} for all points.

plots have been matched at the center of the disk (corresponding to the same point of observation). A similar signal along the central meridian was observed by Kubičela and Karabin (1977), but was misinterpreted due to a lack of knowledge of the limb effect on the disk.

The results of a search for 'limb effect' and 'meridional circulation' using the telluric line λ 6295.962 Å of O_2 suggest that the curves of Figure 9 are real. Five disk points were observed: center of disk, two points placed symmetrically about central meridian on the central swath $0.65R_\odot$ from disk center, and two points placed symmetrically about disk center along the central meridian $0.65R_\odot$ from the center. The points were repeatedly observed over a period of two hours to reduce the noise. A folding operation identical to that used to derive Figure 9 was performed and the resulting three points (1) center of disk, (2) $0.65R_\odot$ from the center toward the equatorial limb, and (3) $0.65R_\odot$ from the center toward the polar limb) had the same signal to within the error of 3 m s^{-1}.

The difference of the two curves of Figure 9 is shown in Figure 10. The zero point can be defined precisely if it is assumed that the center of the disk has zero average velocity with respect to the observer. The velocity difference is interpreted as the line of sight component of a mean meridional circulation directed toward the poles in both hemispheres. The direction of the circulation is opposite to that required to maintain the differential rotation according to the anisotropic eddy viscosity models of Kippenhahn (1963), Cocke (1967), and Köhler (1970). The circulation (~20 m s^{-1}) measured is about a factor of 10 larger than that required by Köhler (1970) to generate differential rotation. However, the giant cell convection models (Gilman, 1972, 1976, 1977) predict a polewards flow for the mean meridional circulation (at the surface). In the giant cell models the differential rotation is generated by Reynolds stresses transporting angular momentum toward the equator. The mean meridional circulation, which is generated as a by-product of the convection, tends to oppose the generation of an equatorial acceleration. The observation of a poleward-directed flow at the surface lends strong support to the giant cell models.

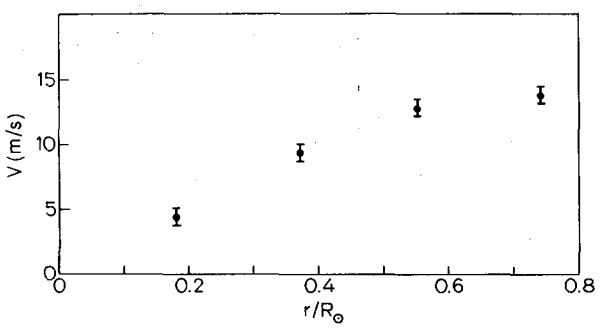

Fig. 10. The difference between the meridional scans and central swath residuals, interpreted as the line of sight component of meridional circulation symmetric across the equator. Positive velocity is directed away from the observer.

Assuming that the flow velocity is horizontal at the photosphere the meridional circulation is derived (Figure 11) as a function of latitude. Because of the large density gradient in the solar atmosphere the upwelling required near the equator to provide the mass flux toward the poles would result in a very small velocity at disk center (on the order of cm s^{-1}) justifying our assumption of zero velocity at disk center. The velocity is seen to be approximately constant over the latitude range 10–50°.

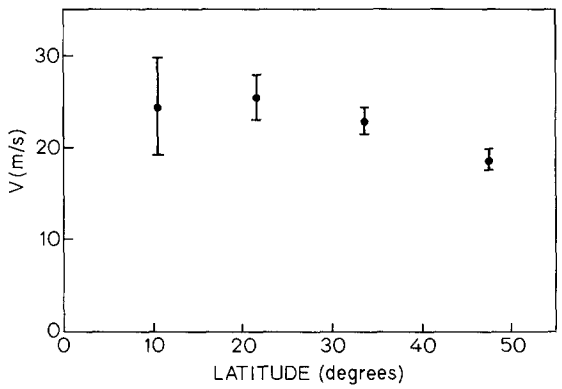

Fig. 11. Assuming the meridional flow is horizontal at the photosphere, the average symmetric component of the meridional circulation has been corrected for the projection of the velocity vector.

4. Summary

The large-scale solar velocity fields have been observed with 3′ resolution using the magnetograph at Stanford. The results are:

(1) The equatorial rotation rate was stable (within 1%) during the time period May 1976–January 1977 at a value of 2.82 μrad s^{-1}.

(2) The limb effect on the disk was measured for the two lines λ 5250 Å and λ 5233 Å of Fe I. For the λ 5250 Å line the profile has a redshift at the center of the disk relative to a position $0.60R_\odot$ from the center of 30 m s^{-1}. For the λ 5233 Å line the center-to-limb variation is qualitatively different, with a redshift at $0.65R_\odot$ from the center relative to disk center of 70 m s^{-1}.

(3) A meridional circulation is found with a flow toward the poles which is approximately constant at 20 m s^{-1} over the latitude range 10–50°. This observation lends support to the giant cell convection models of the differential rotation over the anisotropic eddy viscosity models.

Acknowledgements

This work was supported in part by the Office of Naval Research under Contract N00014-76-C-0207, by the National Aeronautics and Space Administration under

Grant NGR 05-020-559, by the Atmospheric Sciences Section of the National Science Foundation under Grant ATM77-20580 and by the Max C. Fleischmann Foundation.

References

Cocke, W. J.: 1967, *Astrophys. J.* **150**, 1041.
Gilman, P. A.: 1972, *Solar Phys.* **27**, 3.
Gilman, P. A.: 1976, in V. Bumba and J. Kleczek (eds.), 'Basic Mechanisms of Solar Activity', *IAU Symp.* **71**, 207.
Gilman, P. A.: 1977, *Geophys. Astrophys. Fluid Dyn.* **8**, 93.
Hart, M.: 1974, *Astrophys. J.* **187**, 393.
Howard, R.: 1972, *Solar Phys.* **24**, 123.
Howard, R.: 1977, private communication.
Howard, R. and Harvey, J.: 1970, *Solar Phys.* **12**, 23.
Kippenhahn, R.: 1963, *Astrophys. J.* **137**, 664.
Köhler, H.: 1970, *Solar Phys.* **13**, 3.
Kubičela, A. and Karabin, M.: 1977, *Solar Phys.* **52**, 199.
Lites, B. W.: 1972, HAO Research Memorandum No. 185.
Scherrer, P. ., Wilcox, J. M., Svalgaard, L., Duvall, T. L., Jr., Dittmer, P. H., and Gustafson, E. K.: 1977, *Solar Phys.* **54**, 353.
Svalgaard, L., Scherrer, P. H., and Wilcox, J. M., 1979, *Solar Phys.*, in press.